

Quartic Anomalous Couplings in $\gamma\gamma$ Colliders

O. J. P. Éboli*, M. B. Magro†, P. G. Mercadante‡,

Instituto de Física, Universidade de São Paulo,

C.P. 20516, 01452-990 São Paulo, Brazil

S. F. Novaes§

Instituto de Física Teórica, Universidade Estadual Paulista,

Rua Pamplona 145, 01405-900 São Paulo, Brazil

(November 14, 2018)

Abstract

We study the constraints on the vertices $W^+W^-Z\gamma$, $W^+W^-\gamma\gamma$, and $ZZ\gamma\gamma$ that can be obtained from triple-gauge-boson production at the next generation of linear e^+e^- colliders operating in the $\gamma\gamma$ mode. We analyze the processes $\gamma\gamma \rightarrow W^+W^-V$ ($V = Z$, or γ) and show that these reactions increase the potential of e^+e^- machines to search for anomalous four-gauge-boson interactions.

Submitted to Physical Review D1

I. INTRODUCTION

In the next generation of e^+e^- colliders, multiple vector-boson production will provide a crucial test of the gauge structure of the Standard Model (SM), since it will allow the study of the triple and quartic vector-boson couplings. These vertices are strictly constrained by the $SU(2)_L \otimes U(1)_Y$ gauge invariance and any small deviation from the SM predictions spoils the precise cancellation of the high-energy behavior between the various diagrams, giving rise to an anomalous growth of the cross section with energy. Therefore, the careful study of multiple vector-boson production, and consequently of vector-boson self-interactions, can give important clues about the existence of new particles and/or interactions beyond the SM.

The reaction $e^+e^- \rightarrow W^+W^-$ will be accessible at LEP II and some information about the $WW\gamma$ and WWZ vertices will be available in the near future [1]. Nevertheless, we will have to wait for colliders with higher center-of-mass energies in order to produce a final state with three or more gauge bosons and to test the quartic gauge-boson interaction. This will be accomplished at the Next Linear e^+e^- Collider (NLC) [2], which will reach an energy between 500 and 2000 GeV with an yearly integrated luminosity of at least 10 fb^{-1} . An interesting feature of these new machines is the possibility of transforming an electron beam into a photon one through the laser backscattering mechanism [3,4]. This process will allow the NLC to operate in three different modes, e^+e^- , $e\gamma$, and $\gamma\gamma$, opening up the opportunity for a wider search for new physics. However, it is important to point out that the collider can operate in only one of its three modes at a given time, therefore, it is essential to study comparatively the different features of each of these setups.

The triple and quartic gauge-boson vertices, in the framework of gauge theories, have a common origin, and consequently, a universal strength dictated by the gauge symmetry of the model. Notwithstanding, in a more general context, anomalous quartic couplings can arise as the low-energy limit of heavy state exchange, whereas trilinear couplings are modified by integrating out heavy fields. In this sense, it is possible to conceive extensions

of the SM where the trilinear couplings remain unchanged, while the quartic vertices receive new contributions. For instance, the introduction of a new heavy scalar singlet, that interacts strongly with the Higgs sector of the SM, enhances the four vector-boson interaction without affecting either the triple vector-boson couplings or the SM predictions for the ρ parameter [5]. Therefore, the measurement of the three-vector-boson production cross section can provide further non-trivial tests of the SM that are complementary to the analysis of the production of vector-boson pairs.

The cross section for the production of multiple gauge bosons, in the context of the SM, has already been evaluated for e^+e^- colliders operating in the e^+e^- [6,7], $e\gamma$ [8], and $\gamma\gamma$ [9] modes. There has also been some studies of anomalous quartic vertices through the reactions $e^+e^- \rightarrow VVV$ [10,11], $e\gamma \rightarrow VVF$ [12], and $\gamma\gamma \rightarrow VV$ [13], where $V = Z, W^\pm$ or γ and $F = e$ or ν_e . In this work, we analyze the effect of some genuinely anomalous quartic operators, *i.e.* operators which do not modify the trilinear vertices and cannot be bounded by the LEP II measurements. Furthermore, since we are interested in probing these anomalous couplings in a $\gamma\gamma$ collider, we concentrate our analyses on operators that involve at least one photon. We studied the production of three vector bosons in $\gamma\gamma$ collisions through the reactions

$$\gamma + \gamma \rightarrow W^+ + W^- + \gamma, \quad (\text{I})$$

$$\gamma + \gamma \rightarrow W^+ + W^- + Z, \quad (\text{II})$$

in order to impose bounds on the vertices γZW^+W^- , $\gamma\gamma W^+W^-$, and $\gamma\gamma ZZ$. These processes involve only interactions between the gauge bosons, making more evident any deviation from the SM predictions. Moreover, there is no tree-level contribution involving the Higgs boson which evades all the uncertainties coming from the scalar sector, like the Higgs boson mass.

Our results show that the constraint on the anomalous couplings γZW^+W^- , coming from the reaction II, is as restrictive as the one obtained in $e\gamma$ colliders [12] and a factor of

5 better than the one coming from e^+e^- colliders [10,11]. On the other hand, the bounds in the vertices $\gamma\gamma W^+W^-$ and $\gamma\gamma ZZ$, stemming from the processes I and II, are a factor from 2 to 5 better than the ones that can be obtained in an e^+e^- collider, however, they are worse than the ones coming from the direct reaction $\gamma\gamma \rightarrow W^+W^-$ [13].

The next section contains the effective operators that we analyzed and the calculational method employed in this paper. Our results and discussions are presented in Sec. III.

II. EFFECTIVE LAGRANGIANS AND CALCULATIONAL METHOD

In order to construct effective operators associated to exclusively quartic anomalous couplings we employed the formalism of Ref. [14]. We required the existence of a custodial $SU(2)_C$ symmetry, which avoids any contribution to the ρ parameter, and we also demanded that the phenomenological Lagrangians are invariant under local $U(1)_{em}$ symmetry. The lowest order operators that comply with the above requirements, involving at least one photon, are of dimension six [15]: there are two independent C and P conserving operators involving two photons [13]

$$\mathcal{L}_0 = -\frac{\pi\alpha}{4\Lambda^2} a_0 F^{\mu\nu} F_{\mu\nu} W^{(i)\alpha} W_\alpha^{(i)}, \quad (1)$$

$$\mathcal{L}_c = -\frac{\pi\alpha}{4\Lambda^2} a_c F^{\mu\alpha} F_{\mu\beta} W_\alpha^{(i)} W^{(i)\beta}, \quad (2)$$

and one operator exhibiting just one photon [12]

$$\mathcal{L}_n = \frac{\pi\alpha}{4\Lambda^2} a_n \epsilon_{ijk} W_{\mu\alpha}^{(i)} W_\nu^{(j)} W^{(k)\alpha} F^{\mu\nu}, \quad (3)$$

where $W^{(i)}$ is the $SU(2)_C$ triplet and $F^{\mu\nu}$ is the electromagnetic field strength. In terms of the physical fields W^+ , W^- , and Z , the effective Lagrangians (1) and (2) give rise to anomalous $W^+W^-\gamma\gamma$ and $ZZ\gamma\gamma$ couplings, while (3) generates a new $W^+W^-Z\gamma$ vertex. We should notice that the $ZZ\gamma\gamma$ vertex is particularly interesting since it is completely absent in the SM. Moreover, we note that the effective operators (1) and (3) can parametrize the exchange of a neutral scalar particle while the operator (2) corresponds to the exchange of a charged

particle. Therefore, we expect that the characteristic scale of the above interactions is set by the masses of the exchanged states. In the limit of very heavy scalars, the expected values of the coefficients a_i ($i = 0, c, n$) should be in the range of 10^{-2} to 10^{-3} . For the sake of definiteness, our results are presented assuming that $\Lambda = M_W$.

An interesting feature of the above effective Lagrangians is that they will not be directly constrained by LEP II since they do not contribute to triple gauge–boson vertices. In order to obtain some bounds on these couplings at low energies, we must rely on their contribution to one-loop processes. From the analysis of oblique radiative corrections to the Z physics [12], we estimated that $-4.5 < a_0 < 0.64$ and $-11 < a_c < 5.8$ at 1σ level, while the coupling a_n is not constrained at all.

In order to evaluate the triple–vector–boson production at NLC, we assumed that this machine will reach a center–of–mass energy of 500 (1000) GeV with a yearly integrated luminosity of 10 fb^{-1} . The most promising mechanism to generate hard photon beams in an e^+e^- linear collider is laser backscattering. Assuming unpolarized electron and laser beams, the backscattered photon distribution function [4] is

$$F_{\gamma/e}(x, \xi) \equiv \frac{1}{\sigma_c} \frac{d\sigma_c}{dx} = \frac{1}{D(\xi)} \left[1 - x + \frac{1}{1-x} - \frac{4x}{\xi(1-x)} + \frac{4x^2}{\xi^2(1-x)^2} \right], \quad (4)$$

with

$$D(\xi) = \left(1 - \frac{4}{\xi} - \frac{8}{\xi^2} \right) \ln(1 + \xi) + \frac{1}{2} + \frac{8}{\xi} - \frac{1}{2(1 + \xi)^2}, \quad (5)$$

where σ_c is the Compton cross section, $\xi \simeq 4E\omega_0/m_e^2$, m_e and E are the electron mass and energy respectively, and ω_0 is the laser-photon energy. The quantity x represents the ratio between the scattered photon and initial electron energy and its maximum value is

$$x_{\text{max}} = \frac{\xi}{1 + \xi}. \quad (6)$$

In what follows, we assumed that the laser frequency is such that $\xi = 2(1 + \sqrt{2})$, which leads to the hardest possible spectrum of photons with a large luminosity.

The cross section for the triple-vector-boson production via $\gamma\gamma$ fusion can be obtained by folding the elementary cross section for the subprocesses $\gamma\gamma \rightarrow WWV$ ($V = \gamma, Z$) with the photon-photon luminosity ($dL_{\gamma\gamma}/dz$), *i.e.*,

$$d\sigma(e^+e^- \rightarrow \gamma\gamma \rightarrow WWV)(s) = \int_{z_{\min}}^{z_{\max}} dz \frac{dL_{\gamma\gamma}}{dz} d\hat{\sigma}(\gamma\gamma \rightarrow WWV)(\hat{s} = z^2s), \quad (7)$$

where \sqrt{s} ($\sqrt{\hat{s}}$) is the e^+e^- ($\gamma\gamma$) center-of-mass energy, $z^2 = \tau \equiv \hat{s}/s$, and the photon-photon luminosity is

$$\frac{dL_{\gamma\gamma}}{dz} = 2z \int_{z^2/x_{\max}}^{x_{\max}} \frac{dx}{x} F_{\gamma/e}(x, \xi) F_{\gamma/e}(z^2/x, \xi). \quad (8)$$

The analytical calculation of the cross section for the subprocess $\gamma\gamma \rightarrow W^+W^-\gamma$ ($\gamma\gamma \rightarrow W^+W^-Z$) is very lengthy and tedious despite being straightforward. In order to perform these calculations in an efficient and reliable way, we evaluated numerically the helicity amplitudes using the techniques outlined in Ref. [7,16]. The phase space integrations were performed numerically using the Monte Carlo routine VEGAS [17]. As a check of our results, we explicitly verified that the amplitudes were Lorentz and $U(1)_{em}$ invariant and that the kinematic distributions for W^+ and W^- coincided.

III. RESULTS AND DISCUSSION

The total cross sections for the processes I and II are quadratic functions of the anomalous couplings a_i , *i.e.*

$$\sigma_{\text{tot}} = \sigma_{\text{sm}} + a_i \sigma_{\text{int}}^i + a_i^2 \sigma_{\text{ano}}^i, \quad (9)$$

where σ_{sm} stands for the SM cross section [9] and σ_{int}^i (σ_{ano}^i) is the interference (pure anomalous) contribution. We evaluated the cross sections involved in Eq. (9), imposing that the polar angles of the produced vector bosons with the beam pipe are larger than 10° and assuming $\Lambda = M_W$. For the process I, we also introduced a cut on the photon transverse momentum, $p_T^\gamma > 10$ (20) GeV, not only to guarantee that our results are free of infrared divergences but also to mimic the performance of a typical electromagnetic calorimeter. In

Table I, we present our results assuming in each case that only one anomalous coupling is nonvanishing.

In order to quantify the effect of the new couplings, we defined the statistical significance S of the anomalous signal

$$S = \frac{|\sigma_{tot} - \sigma_{sm}|}{\sqrt{\sigma_{sm}}} \sqrt{\mathcal{L}}, \quad (10)$$

which can be easily evaluated using the parametrization (9) with the coefficients given in Table I. We list in Table II the values of the anomalous couplings that correspond to a 3σ effect in the total cross section for the different processes, assuming an integrated luminosity $\mathcal{L} = 10 \text{ fb}^{-1}$ for the correspondent e^+e^- collider. It is interesting to point out that the most stringent bounds come from the process I and that our results are quite insensitive to different choices of the angular and p_T^γ cuts, as we can learn from Table II.

We can see from Table II that our 3σ limits for the coupling a_n are a factor of 3 better than the limits obtained in e^+e^- collisions [10,11], while they are of the same order of the ones originating from an $e\gamma$ machine [12]. The $\gamma\gamma$ mode of the NLC is more efficient for studying this anomalous quartic coupling since it leads to cross sections for the production of three vector bosons that is more than one order of magnitude larger than the ones for a conventional e^+e^- collider with $\sqrt{s} \geq 500$ [9].

The limits on the anomalous coupling a_c that can be established through the triple gauge-boson production are one order of magnitude better than the ones coming from the e^+e^- mode and are comparable to the constraints that can be obtained in the $e\gamma$ mode. However, the bounds shown in Table II are a factor of 2 weaker than the ones obtained from the direct reaction $\gamma\gamma \rightarrow W^+W^- (ZZ)$, since the triple gauge-boson production is a higher order process in α_{em} . Our limits on the coupling a_0 are slightly better than the ones arising from the e^+e^- mode, while they are almost one order of magnitude worse than the ones obtained in $e\gamma$ [12] or direct $\gamma\gamma \rightarrow W^+W^- (ZZ)$ [13] collisions.

The kinematical distributions of the final state particles can be used, at least in principle, to increase the sensitivity of the $\gamma\gamma$ reactions to the anomalous couplings, improving con-

sequently the bounds on the new interactions. More than that, they could furnish further information that would allow us to distinguish among the different anomalous interactions. In Figs. 1 to 4, we exhibit some representative distributions for the processes I and II, adopting the values of the anomalous coupling constants that lead to a 3σ deviation in the total cross section.

We present in Fig. 1 the normalized $\cos\theta_{W^\pm}$ distribution for the production of $W^+W^-\gamma$, where θ_{W^\pm} is polar angle of the vector boson with respect to the beam pipe. From this figure, we can see that the anomalous W distributions differ from the SM one. For instance, we can identify the cases with negative values of a_0 and a_c , but we cannot discriminate between the positive values of these anomalous couplings. Moreover, it is interesting to notice that the anomalous couplings enhance the production of W^\pm in the central region of the detector, where they can be more easily reconstructed.

Figure 2 contains the normalized distribution for the invariant mass (M) of vector–boson pairs W^+W^- for the process I. Here we can observe that the presence of the anomalous interactions increases the invariant mass of the W^+W^- pairs since the new couplings are proportional to the photon momentum. Furthermore, this distribution allows us to separate the negative a_0 and a_c couplings, while the positive values of the anomalous couplings lead to distributions similar to the SM ones. We notice in our analyses that the distributions involving photons are less sensitive to the anomalous couplings than the W^\pm ones.

Although the process $\gamma\gamma \rightarrow W^+W^-Z$ has a lower sensitivity, when compared with the $W^+W^-\gamma$ production, it exhibits some interesting features, as can be seen from Figs. 3 and 4. We show in Fig. 3 the normalized Z transverse momentum distributions for the process II using the a_0 , a_c , and a_n anomalous couplings. We can learn from this figure that the anomalous couplings favor the Z 's to have a higher p_T since the momentum dependence of the anomalous vertices enhances their contribution at higher energies. Once again, we can distinguish between the different anomalous interactions provided the couplings a_0 and a_c are negative, since these couplings lead to larger purely anomalous contributions. It is interesting to remark that our analyses show that the $p_T^{W^\pm}$ distribution does not allow us to

separate clearly the different anomalous interactions.

In Fig. 4, we show the W^\pm rapidity distributions for the process II. The anomalous interactions lead to a more copious production of W^\pm in the central region and it is also possible to have an indication of which effective interaction is responsible for the departure from the SM predictions. We found out that, as happened in $W^+W^-\gamma$ process, it is not possible to distinguish between the anomalous interactions through the rapidity distribution of the neutral vector bosons.

The bottom line of this work is that the study of the production of $W^+W^-\gamma$ and W^+W^-Z in a $\gamma\gamma$ collider will be able to increase the potential of e^+e^- machines to search for anomalous four-gauge-boson interactions. Furthermore, the kinematical distributions of the final state particle can also help to distinguish between some of these interactions.

ACKNOWLEDGMENTS

This work was partially supported by Conselho Nacional de Desenvolvimento Científico e Tecnológico (CNPq), and by Fundação de Amparo à Pesquisa do Estado de São Paulo (FAPESP).

APPENDIX:

We collect in this appendix the expressions for anomalous contributions to the the amplitudes of the processes $\gamma\gamma \rightarrow W^+W^-V$, with $V = Z$ or γ . The standard model expressions can be found in Ref. [9]. The momenta and polarizations of the initial photons were denoted by (k_1, k_2) and $[\epsilon_\mu(k_1), \epsilon_\nu(k_2)]$, while the momenta and polarizations of the final state W^+ , W^- and V are given by (p_+, p_-, k_3) and $[\epsilon_\alpha(p_+), \epsilon_\beta(p_-), \epsilon_\gamma(k_3)]$ respectively. The amplitude of these processes can be written as

$$\mathcal{M}_i = G_V \epsilon_\mu(k_1) \epsilon_\nu(k_2) \epsilon_\alpha(p_+) \epsilon_\beta(p_-) \epsilon_\gamma(k_3) \left[M_{\text{sm}}^{\mu\nu\alpha\beta\gamma} + M_{\text{ano}}^{\mu\nu\alpha\beta\gamma}(i) \right], \quad (\text{A1})$$

where M_{sm} is the standard model invariant amplitude, and $M_{\text{ano}}(i)$, $i = a_0, a_c, a_n$, represents the different anomalous contributions. The factor G_V depends upon the process under consideration: $G_V = e^3$ for the production of $W^+W^-\gamma$ and $G_V = e^3 \cot^2 \theta_W$ for the production of W^+W^-Z .

We can write a compact expression for the anomalous amplitudes of the process (I), in the form

$$\begin{aligned} (M_{\text{ano}}^\gamma)^{\mu\nu\alpha\beta\gamma}(a_0) &= [M_1(a_0) + M_2(a_0) + M_3(a_0) + M_4(a_0)]^{\mu\nu\alpha\beta\gamma} , \\ (M_{\text{ano}}^\gamma)^{\mu\nu\alpha\beta\gamma}(a_c) &= [M_1(a_c) + M_2(a_c) + M_3(a_c) + M_4(a_c)]^{\mu\nu\alpha\beta\gamma} , \end{aligned} \quad (\text{A2})$$

while for the process (II) we have

$$\begin{aligned} (M_{\text{ano}}^Z)^{\mu\nu\alpha\beta\gamma}(a_0) &= [M_3(a_0) + M_4(a_0) + M_5(a_0)]^{\mu\nu\alpha\beta\gamma} , \\ (M_{\text{ano}}^Z)^{\mu\nu\alpha\beta\gamma}(a_c) &= [M_3(a_c) + M_4(a_c) + M_5(a_c)]^{\mu\nu\alpha\beta\gamma} , \\ (M_{\text{ano}}^Z)^{\mu\nu\alpha\beta\gamma}(a_n) &= [M_1(a_n) + M_2(a_n) + M_6(a_n)]^{\mu\nu\alpha\beta\gamma} , \end{aligned} \quad (\text{A3})$$

with

$$\begin{aligned} M_1^{\mu\nu\alpha\beta\gamma}(i) &= \Delta^{\beta\nu\xi}(-p_-, k_2) D_{\xi\lambda}^W(k_2 - p_-) \Gamma_{(i)}^{\lambda\alpha\mu\gamma}(k_1, -k_3, k_2 - p_-, -p_+) + [k_1 \leftrightarrow 2 ; \mu \leftrightarrow \nu] , \\ M_2^{\mu\nu\alpha\beta\gamma}(i) &= \Delta^{\mu\alpha\xi}(k_1, -p_+) D_{\xi\lambda}^W(k_1 - p_+) \Gamma_{(i)}^{\lambda\beta\nu\gamma}(k_2, -k_3, -p_-, k_1 - p_+) + [k_1 \leftrightarrow 2 ; \mu \leftrightarrow \nu] , \\ M_3^{\mu\nu\alpha\beta\gamma}(i) &= \Delta^{\alpha\gamma\xi}(p_+, k_3) D_{\xi\lambda}^W(p_+ + k_3) \Gamma_{(i)}^{\lambda\beta\nu\mu}(k_1, k_2, 0, 0) , \\ M_4^{\mu\nu\alpha\beta\gamma}(i) &= \Delta^{\gamma\beta\xi}(k_3, p_-) D_{\xi\lambda}^W(-p_- - k_3) \Gamma_{(i)}^{\lambda\alpha\nu\mu}(k_1, k_2, 0, 0) , \\ M_5^{\mu\nu\alpha\beta\gamma}(i) &= \frac{1}{\cos^2 \theta_W} \Delta^{\alpha\beta\xi}(p_-, p_+) D_{\xi\lambda}^Z(p_+ + p_-) \Gamma_{(i)}^{\lambda\gamma\nu\mu}(k_1, k_2, 0, 0) , \\ M_6^{\mu\nu\alpha\beta\gamma}(i) &= -\frac{a_n \sin \theta_W}{16 \cos \theta_W \Lambda^2} \left(2p_2^\mu g^{\alpha\beta} g^{\nu\gamma} - 2p_2^\gamma g^{\alpha\beta} g^{\mu\nu} - p_2^\mu g^{\alpha\gamma} g^{\nu\beta} + p_2^\beta g^{\mu\nu} g^{\alpha\gamma} \right. \\ &\quad \left. - p_2^\mu g^{\beta\gamma} g^{\alpha\nu} + p_2^\alpha g^{\mu\nu} g^{\beta\gamma} - p_2^\alpha g^{\mu\beta} g^{\nu\gamma} + p_2^\gamma g^{\mu\beta} g^{\nu\alpha} - p_2^\beta g^{\mu\alpha} g^{\nu\gamma} + p_2^\gamma g^{\mu\alpha} g^{\nu\beta} + 1 \leftrightarrow 2 \right) . \end{aligned} \quad (\text{A4})$$

In Eq. (A4), $D_{\xi\lambda}^V$, $V = W, Z$, represents the vector boson propagator in the unitary gauge, Δ is the usual triple-gauge-boson vertex function

$$\Delta^{\alpha\beta\gamma}(q_1, q_2) = i \left[(2q_1 + q_2)^\beta g^{\alpha\gamma} - (2q_2 + q_1)^\alpha g^{\beta\gamma} + (q_2 - q_1)^\gamma g^{\beta\alpha} \right] , \quad (\text{A5})$$

and, $\Gamma_{(i)}$ are the different four-gauge-boson couplings for the anomalous interactions

$$\Gamma_{(a_0)}^{\mu\nu\alpha\beta}(q_1, q_2, q_3, q_4) = i \frac{a_0}{2\Lambda^2} g^{\mu\nu} \left[g^{\alpha\beta} (q_1 \cdot q_2) - q_2^\alpha q_1^\beta \right], \quad (\text{A6})$$

$$\Gamma_{(a_c)}^{\mu\nu\alpha\beta}(q_1, q_2, q_3, q_4) = i \frac{a_c}{8\Lambda^2} \left[(q_1 \cdot q_2) (g^{\mu\alpha} g^{\nu\beta} + g^{\mu\beta} g^{\alpha\nu}) + g^{\alpha\beta} (q_1^\mu q_2^\nu + q_2^\mu q_1^\nu) - q_1^\beta (g^{\alpha\mu} q_2^\nu + g^{\alpha\nu} q_2^\mu) - q_2^\alpha (g^{\beta\mu} q_1^\nu + g^{\beta\nu} q_1^\mu) \right], \quad (\text{A7})$$

$$\Gamma_{(a_n)}^{\mu\nu\alpha\beta}(q_1, q_2, q_3, q_4) = \frac{a_n \sin \theta_W}{16 \cos \theta_W^2 \Lambda^2} \left\{ \begin{aligned} &g^{\mu\beta} [g^{\nu\alpha} q_1 \cdot (q_2 - q_3) - q_1^\nu (q_2 - q_3)^\alpha] \\ &- g^{\nu\beta} [g^{\mu\alpha} q_1 \cdot (q_2 - q_4) - q_1^\mu (q_2 - q_4)^\alpha] \\ &+ g^{\mu\nu} [g^{\alpha\beta} q_1 \cdot (q_3 - q_4) - (q_3 - q_4)^\alpha q_1^\beta] \\ &- q_2^\mu (g^{\alpha\nu} q_1^\beta - g^{\alpha\beta} q_1^\nu) + q_2^\nu (g^{\alpha\mu} q_1^\beta - g^{\alpha\beta} q_1^\mu) \\ &- q_4^\beta (g^{\alpha\mu} q_1^\nu - g^{\alpha\nu} q_1^\mu) + q_3^\beta (g^{\alpha\nu} q_1^\mu - g^{\alpha\mu} q_1^\nu) \\ &- q_3^\nu (g^{\alpha\beta} q_1^\mu - g^{\alpha\mu} q_1^\beta) + q_4^\mu (g^{\alpha\beta} q_1^\nu - g^{\alpha\nu} q_1^\beta) \end{aligned} \right\}. \quad (\text{A8})$$

The amplitude M_5 comes from the new anomalous vertex $\gamma\gamma ZZ$, and \mathcal{L}_n gives rise to a five-vertex $\gamma\gamma W^+W^-Z$ represented by M_6 , which is necessary to preserve the gauge invariance of the amplitude.

REFERENCES

- * Electronic address: eboli@snfma1.if.usp.br (internet) or 47602::eboli (decnet).
- † Electronic address: magro@snfma1.if.usp.br (internet) or 47602::magro (decnet).
- ‡ Electronic address: mercadan@snfma1.if.usp.br (internet) or 47602::mercadante (decnet).
- § Electronic address: novaes@vax.ift.unesp.br (internet) or 47553::novaes (decnet).
- [1] K. Hagiwara, R. D. Peccei, D. Zeppenfeld, and K. Hikasa, Nucl. Phys. **B282**, 253 (1987); Proceedings of the ECFA Workshop on LEP200, CERN Report 87-08, ECFA Report 87/108, ed. A. Böhm and W. Hoogland, Aachen 1987.
- [2] R. B. Palmer, Annu. Rev. Nucl. Part. Sci. **40**, 529 (1990).
- [3] F. R. Arutyunian, and V. A. Tumanian, Phys. Lett. **4**, 176 (1963); R. H. Milburn, Phys. Rev. Lett. **10**, 75 (1963); see also C. Akerlof, University of Michigan Report No. UMHE 81-59 (1981), unpublished.
- [4] I. F. Ginzburg, G. L. Kotkin, V. G. Serbo, and V. I. Telnov, Nucl. Instrum. Methods **205**, 47 (1983); **219**, 5 (1984); V. I. Telnov, Nucl. Instrum. Methods **A294**, 72 (1990).
- [5] A. Hill and J. J. van der Bij, Phys. Rev. **D36**, 3463 (1987).
- [6] V. Barger and T. Han, Phys. Lett. **212B**, 117 (1988); A. Tofighi-Niaki and J. F. Gunion, Phys. Rev. **D39**, 720 (1989).
- [7] V. Barger, T. Han, and R. J. N. Phillips, Phys. Rev. **D39**, 146 (1989).
- [8] K. Cheung, Nucl. Phys. **B403**, 572 (1993).
- [9] M. Baillargeon and F. Boudjema, Phys. Lett. **B317**, 371 (1993); O. J. P. Éboli *et al*, Phys. Rev. **D50**, 5591 (1994).
- [10] G. Bélanger and F. Boudjema, Phys. Lett. **B288**, 201 (1992).

- [11] G. A. Leil and W. J. Stirling, preprint DTP/94/10 (hep-ph/9406317) june 1994.
- [12] O. J. P. Éboli, M. C. Gonzalez-Garcia, and S. F. Novaes, Nucl. Phys. **B411**, 381 (1994).
- [13] G. Bélanger and F. Boudjema, Phys. Lett. **B288**, 210 (1992).
- [14] M. Kuroda et al., Nucl. Phys. **B284** (1987) 271; M. Kuroda, F. M. Renard, and D. Schildknecht, Phys. Lett. **B183**, 366 (1987).
- [15] These interactions can be written as chiral Lagrangians. See, for instance, M. Baillargeon, G. Bélanger, and F. Boudjema preprint ENSLAPP-A-473/94 (hep-ph/9405359).
- [16] K. Hagiwara and D. Zeppenfeld, Nucl. Phys. **B274**, 1 (1986).
- [17] G. P. Lepage, J. Comp. Phys. **27**, 192 (1978).

FIGURES

FIG. 1. Normalized angular distributions of the W^\pm bosons with the beam pipe (process I) for $\sqrt{s} = 500$ GeV and $p_T^\gamma > 10$ GeV. The dotted line is the SM result and the dashed line stands for both $a_0 = 0.062$ and $a_c = 0.17$, while the solid (dot-dashed) line represents the results for $a_0 = -0.17$ ($a_c = -0.83$).

FIG. 2. Normalized invariant mass distribution for the W^+W^- pairs (process I) for $\sqrt{s} = 500$ GeV and $p_T^\gamma > 10$ GeV. The dotted line is the SM result, and the dashed (solid) line represents the results for $a_0 = -0.17$ ($a_c = -0.83$). The results for $a_0 = 0.062$ and $a_c = 0.17$ cannot be distinguished from the SM one.

FIG. 3. Normalized transverse momentum distribution of the Z boson (process II) at $\sqrt{s} = 500$ GeV. The histogram is the SM result, the dashed line stands for $a_0 = 0.11$ and $a_c = 0.32$, the dotted (dot-dashed) line represents the results for $a_0 = -0.34$ ($a_c = -1.4$), and the solid line stands for $a_n = 1.55$.

FIG. 4. Normalized rapidity distribution of the W^\pm bosons (process II) at $\sqrt{s} = 500$ GeV. The conventions are the same as in Fig. 3. It is useful to observe that the dotted line coincides with the dashed one.

TABLES

	$WW\gamma$				WWZ	
	$P_T^\gamma > 10 \text{ GeV}$		$P_T^\gamma > 20 \text{ GeV}$			
	0.5 TeV	1 TeV	0.5 TeV	1 TeV	0.5 TeV	1 TeV
\sqrt{s}						
$\sigma_{\text{sm}} (\times 10^2 \text{ fb})$	2.55	7.83	1.45	5.21	1.90×10^{-1}	2.38
$\sigma_{\text{int}}^0 (\times 10^2 \text{ fb})$	1.53	9.81	9.50×10^{-1}	7.25	2.50×10^{-1}	6.13
$\sigma_{\text{ano}}^0 (\times 10^2 \text{ fb})$	1.44×10^1	3.25×10^3	8.57	2.29×10^3	1.08	1.02×10^3
$\sigma_{\text{int}}^c (\times 10^2 \text{ fb})$	7.10×10^{-1}	4.65	3.20×10^{-1}	2.68	1.00×10^{-1}	2.74
$\sigma_{\text{ano}}^c (\times 10^2 \text{ fb})$	1.07	2.33×10^2	6.00×10^{-1}	1.63×10^2	9.00×10^{-2}	7.61×10^1
$\sigma_{\text{int}}^n (\times 10^2 \text{ fb})$	—	—	—	—	0	0
$\sigma_{\text{ano}}^n (\times 10^2 \text{ fb})$	—	—	—	—	1.70×10^{-1}	5.51

TABLE I. Cross sections σ_{sm}^i , σ_{int}^i , and σ_{ano}^i , **assuming** $\Lambda = M_W$.

	$WW\gamma$				WWZ	
	$p_T^\gamma > 10 \text{ GeV}$		$p_T^\gamma > 20 \text{ GeV}$			
	0.5 TeV	1 TeV	0.5 TeV	1 TeV	0.5 TeV	1 TeV
a_0	(-0.17, 0.062)	(-0.011, 0.0077)	(-0.18, 0.072)	(-0.011, 0.0083)	(-0.34, 0.11)	(-0.015, 0.0094)
a_c	(-0.83, 0.17)	(-0.045, 0.025)	(-0.78, 0.24)	(-0.046, 0.029)	(-1.4, 0.32)	(-0.065, 0.029)
a_n	—	—	—	—	(-1.6, 1.6)	(-0.16, 0.16)
$ \Delta\sigma $	15	26	12	22	4.1	14

TABLE II. Allowed intervals of a_i corresponding to an effect smaller than 3σ in the total cross section. We also exhibit the difference ($\Delta\sigma$) between the anomalous cross sections and the SM ones in fb for a 3σ effect.

This figure "fig1-1.png" is available in "png" format from:

<http://arxiv.org/ps/hep-ph/9503432v1>

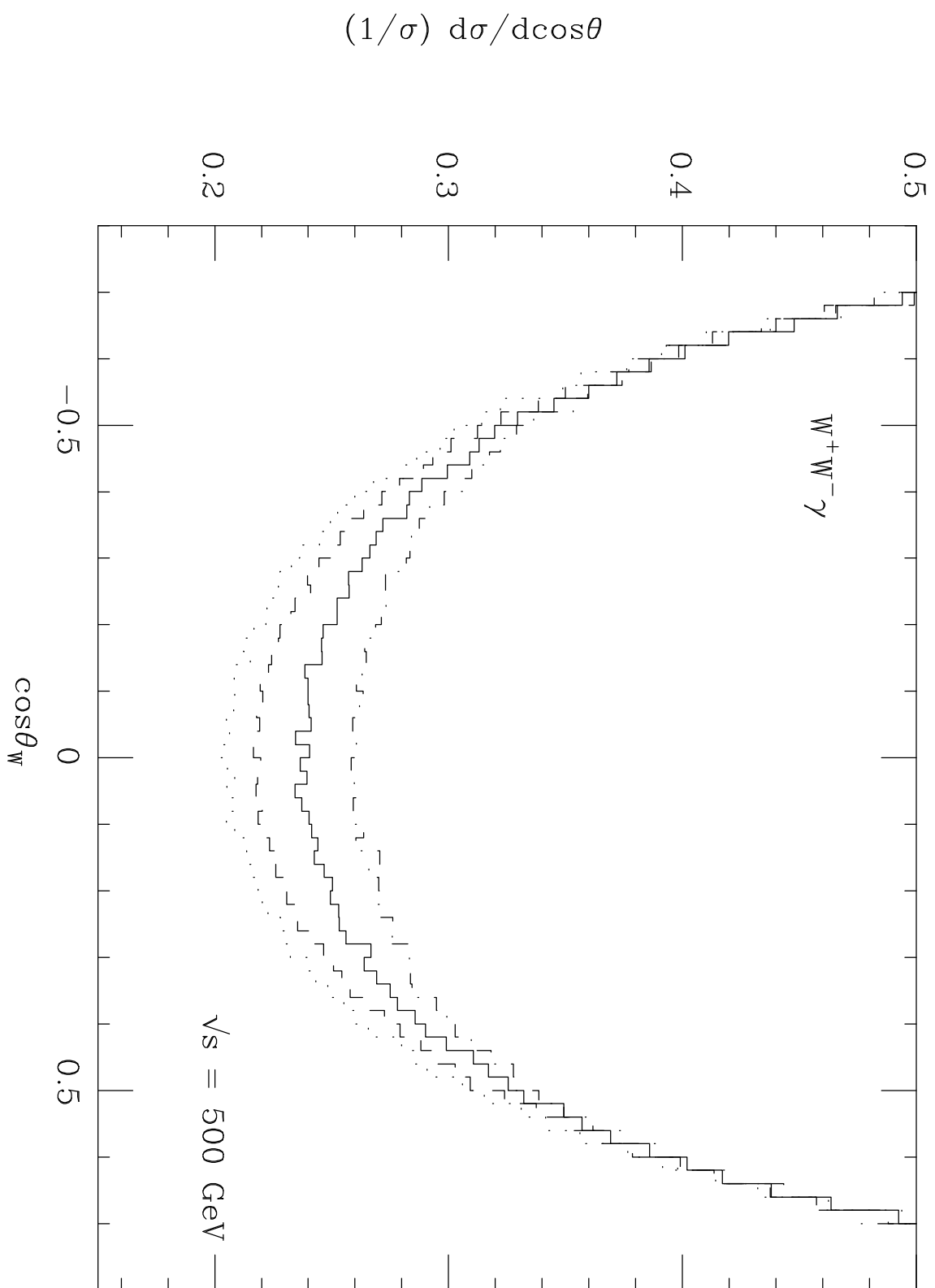


Fig. 1

This figure "fig1-2.png" is available in "png" format from:

<http://arxiv.org/ps/hep-ph/9503432v1>

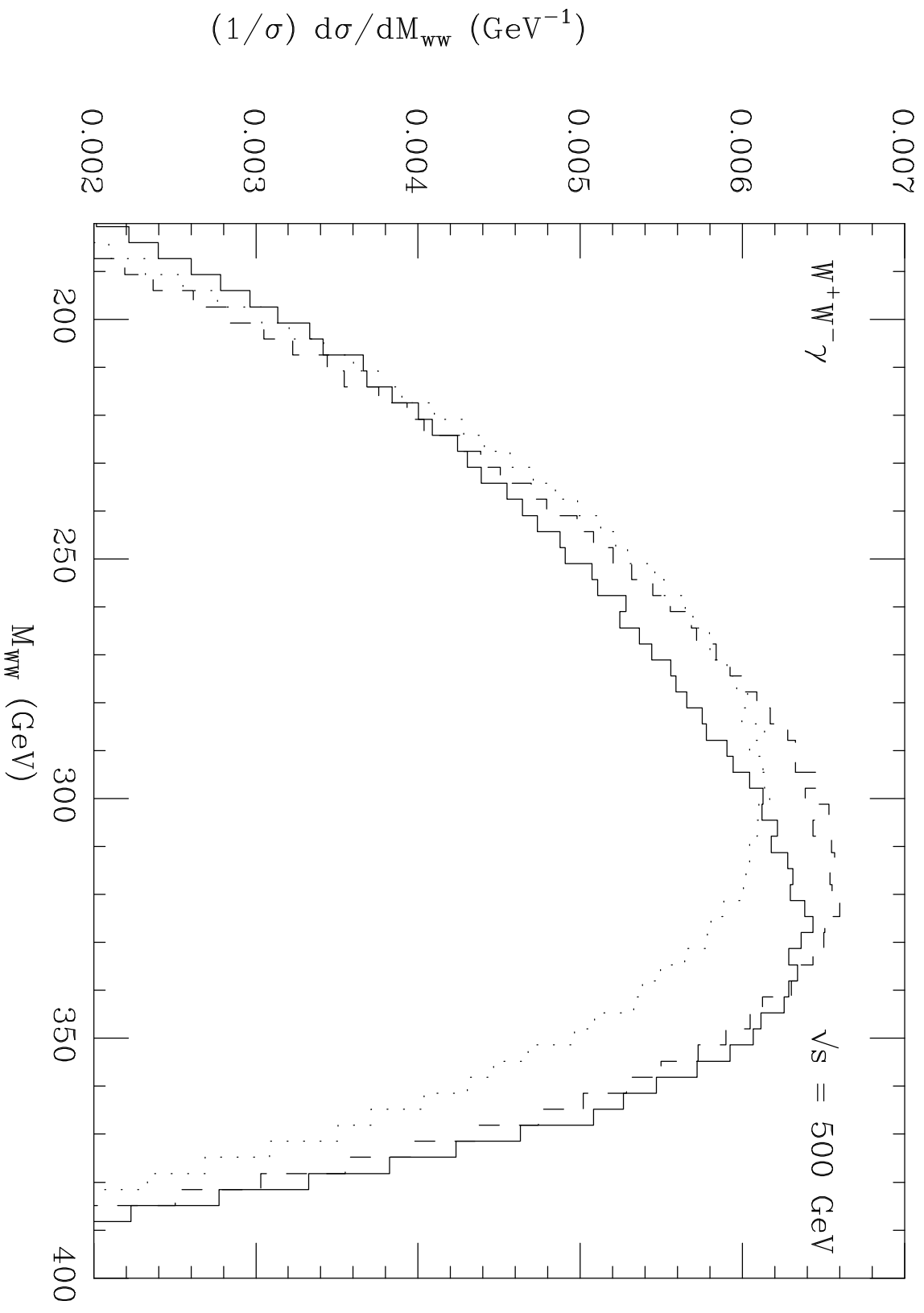


Fig. 2

This figure "fig1-3.png" is available in "png" format from:

<http://arxiv.org/ps/hep-ph/9503432v1>

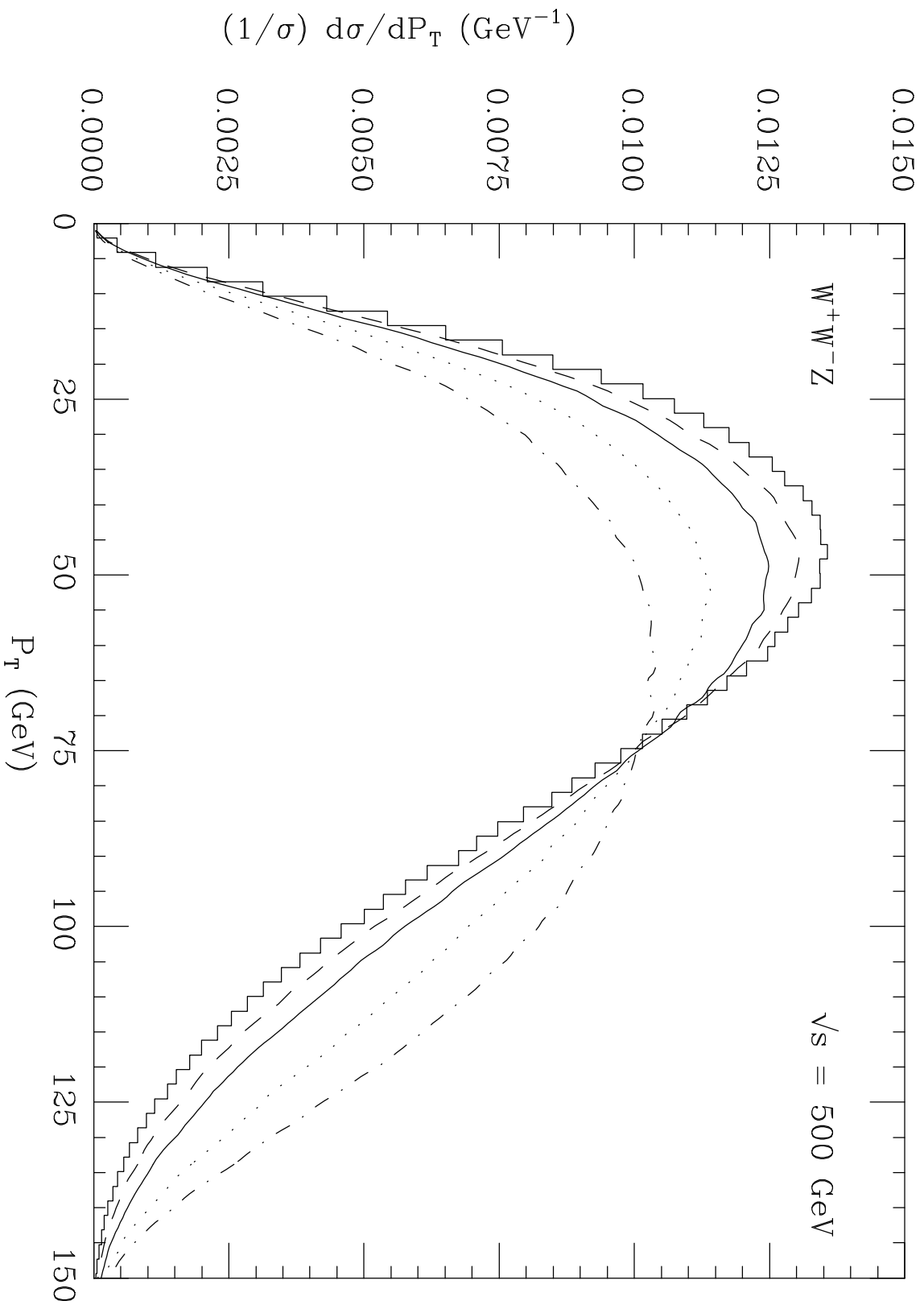


Fig. 3

This figure "fig1-4.png" is available in "png" format from:

<http://arxiv.org/ps/hep-ph/9503432v1>

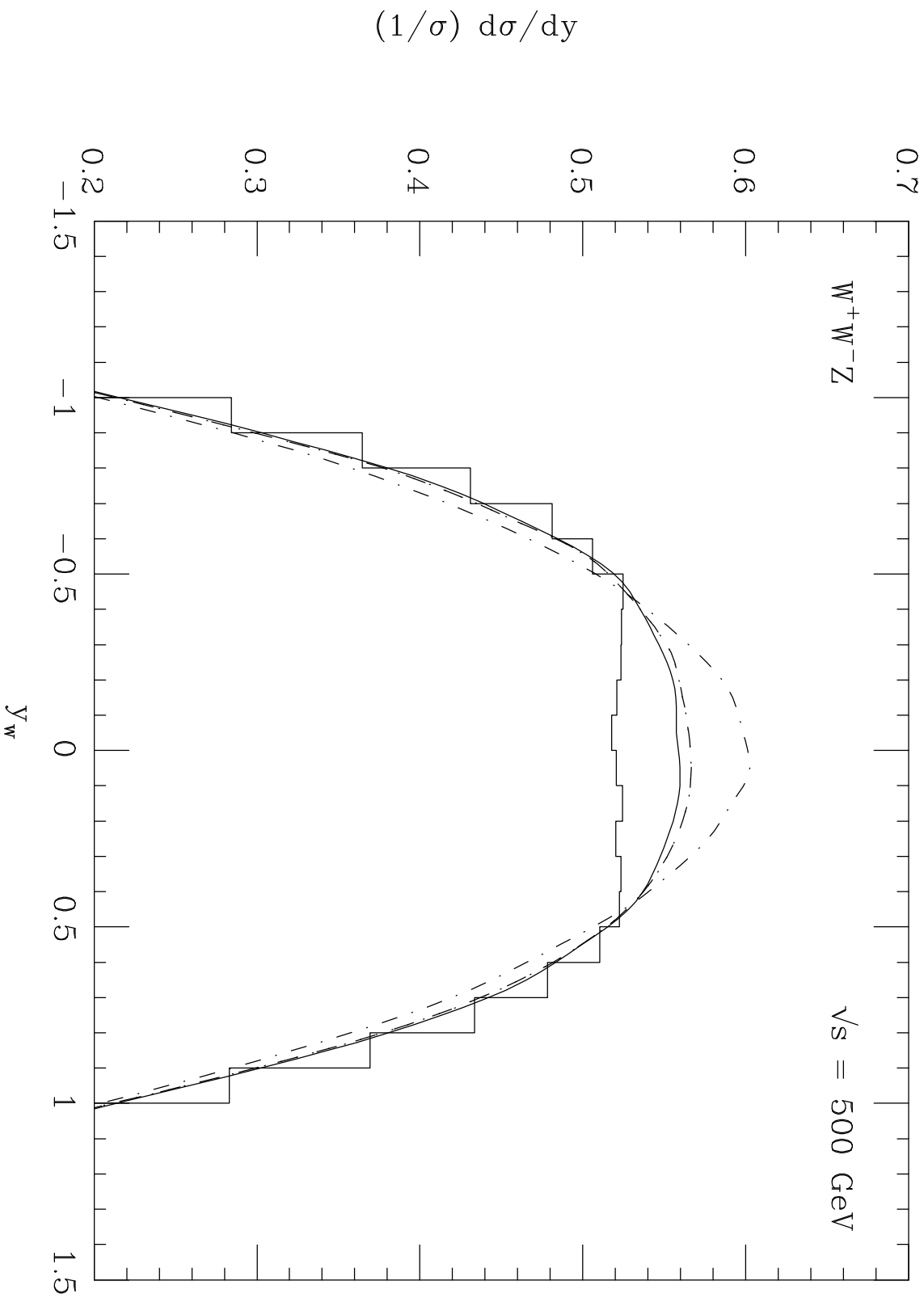


Fig. 4